

Opportunities of Hybrid Model-based Reinforcement Learning for Cell Therapy Manufacturing Process Development and Control

Hua Zheng^a, Wei Xie^{a,*}, Keqi Wang^a and Zheng Li^c

^aDepartment of Mechanical and Industrial Engineering, Northeastern University, Boston, MA 02115, USA

^cGenentech, Inc., South San Francisco, CA, USA

ARTICLE INFO

Keywords:

Cell therapy manufacturing
Biomanufacturing process hybrid model
latent State
reinforcement learning
stochastic decision process
model estimation uncertainty
stochastic process optimization

ABSTRACT

Driven by the key challenges of cell therapy manufacturing, including high complexity, high uncertainty, and very limited process data, we propose a stochastic optimization framework named “hybrid-RL” to efficiently guide process development and control. We first create the bioprocess probabilistic knowledge graph that is a hybrid model characterizing the understanding of biomanufacturing process mechanisms and quantifying inherent stochasticity, such as batch-to-batch variation and bioprocess noise. It can capture the key features, including nonlinear reactions, time-varying kinetics, and partially observed bioprocess state. This hybrid model can leverage on existing mechanistic models and facilitate the learning from process data. Given limited process data, a computational sampling approach is used to generate posterior samples quantifying the model estimation uncertainty. Then, we introduce hybrid model-based Bayesian reinforcement learning (RL), accounting for both inherent stochasticity and model uncertainty, to guide optimal, robust, and interpretable decision making, which can overcome the key challenges of cell therapy manufacturing. In the empirical study, cell therapy manufacturing examples are used to demonstrate that the proposed hybrid-RL framework can outperform the classical deterministic mechanistic model assisted process optimization.

1. Introduction

The past decade has seen unparalleled growth in the field of cell therapies used to treat and prevent diseases, such as cancers, cardiovascular and hematologic diseases, through the pharmacological, immunological, or metabolic actions of cells or tissues (Wang et al., 2021b; Hanna et al., 2016). Kymriah (tisagenlecleucel) made history in August 2017 when it became the world’s first approved chimeric antigen receptor (CAR) T-cell therapy. The projected worth of the cellular therapy market is \$8.21 billion in 2025 (Fiorenza et al., 2020).

Cell therapy manufacturing faces critical challenges, including high complexity, high variability, and limited process data. The productivity and functional identity of cell products are sensitive to cell culture conditions. Improper cultivation can not only hinder yield, but can result in heterogeneously differentiated cell populations or contamination, which could give rise to potential tumor or teratoma formulation in cell graft recipients. In addition, since cell therapies become more and more personalized, there are often very limited data for process development and control. The seed cells can be extracted and isolated from individual patients and donors, which leads to high variability.


For biochemical processes, the laws of biophysical chemistry often allow us to construct mechanistic models. However, existing mechanistic models often ignore the impact from various sources of biomanufacturing process inherent stochasticity. For example, although batch-to-batch variation and bioprocess noise are often dominant sources of process variation (Mockus et al., 2015), biochemical kinetics

literature rarely incorporates them into the ordinary/partial differential equation (ODE/PDE) based mechanistic models. In a study on the microbial cell-to-cell phenotypic diversity, Vasdekis et al. (2015) identified the intracellular production fluctuations as one of the major sources of the bioprocessing noise. In addition, raw material variability is another critical source of uncertainty impacting cell cultures (Dickens et al., 2018). Correctly quantifying the impact of all sources of variations is critically important to support reliable process optimization.

There are two types of uncertainty impacting on cell therapy manufacturing process optimization, including (1) inherent stochasticity from raw materials, critical process parameters (CPPs), and other uncontrolled variables (such as contamination); and (2) model estimation uncertainty incurred because the bioprocess model is an approximation of the real process. The process inherent stochasticity can be controlled by improving the identification and specification of CPPs. The model uncertainty can be reduced by collecting more informative process observations. Given very limited process data, the model uncertainty is often large. *Therefore, correctly quantifying all sources of uncertainty can facilitate learning and support robust, automatic, and reliable biomanufacturing process decision making.*

Various process analytical technologies (PATs) and control methodologies have been proposed to guide biomanufacturing process decision making and variation control; see the review in Steinwandter et al. (2019). The existing control strategies are often derived based on deterministic first-principle models. They often overlook bioprocess stochastic uncertainty and model uncertainty. Markov decision processes (MDP) and reinforcement learning (RL) based process optimization approaches draw increasing attentions in the recent studies (Spielberg et al., 2017, 2020; Martagan

*Corresponding author

 w.xie@northeastern.edu (W. Xie)

ORCID(s): 0000-0001-9563-4927 (W. Xie)

et al., 2018; Liu et al., 2013). However, the existing bioprocess modeling, analytics, and optimization approaches have several key limitations. First, mechanistic models, in which conservation equations, kinetics, thermodynamics, and transport phenomena are modeled by ordinary or partial differential equations (ODEs/PDEs), are usually deterministic, while real bioprocess operations are stochastic. Second, existing MDP and RL approaches often focus on developing general methodologies without incorporating the prior knowledge on bioprocessing mechanisms, which limits their performance, interpretability, and adoption.

Driven by the critical challenges in cell therapy manufacturing, we propose a stochastic optimization framework named “hybrid-RL” building on bioprocess probabilistic knowledge graph (KG) in conjunction with model-based RL to efficiently guide process development and control. The core contributions of this paper are summarized as follows.

- We first create a KG hybrid model characterizing the risk- and science-based understanding of biomanufacturing process mechanisms. It quantifies cell therapy manufacturing inherent stochasticity, including batch-to-batch variation and bioprocess noise. This hybrid model can leverage information from existing mechanistic models and further facilitate the learning from process data. Comparing to existing approaches (Zheng et al., 2021b), the proposed knowledge graph hybrid model can capture the key features of bioprocesses, including nonlinear reactions, time-varying dynamics, and partially observed state.
- Given very limited process observations, the Bayesian inference is used to derive a posterior distribution of the hybrid model. We use a computational sampling approach to generate posterior samples quantifying model estimation uncertainty, and further construct the predictive distribution accounting for both inherent stochasticity and model uncertainty.
- We then introduce the hybrid model-based Bayesian reinforcement learning approach (call “hybrid-RL”) to find optimal, robust, and interpretable decision making and control policies, which can overcome the key challenges of cell therapy manufacturing. This hybrid model-based optimization scheme can provide an insightful prediction on how the effects of decision inputs propagate through bioprocess mechanism pathways and impact on integrated manufacturing output trajectory dynamics and variation.
- We demonstrate the opportunities of utilizing the proposed hybrid model-based RL for cell therapy manufacturing process optimization. The empirical study results show that the proposed framework has a great potential to outperform the classical approach.

The remainder of the paper is organized as follows. We give a brief review of the biomanufacturing process modeling and optimization approaches in Section 2. We provide

the problem description and summarize the proposed framework in Section 3. Then, we present a probabilistic KG hybrid model and use the approximate Bayesian computation (ABC) approach to generate posterior samples quantifying model uncertainty and facilitate the bioprocess mechanisms learning in Section 4. We further provide the hybrid model based Bayesian RL in Section 5. We conduct the empirical study of the erythroblast cell culture optimization examples in Section 6 and conclude the paper in Section 7.

2. Literature Review

Bioprocess Modeling and Analysis: In classic biomanufacturing literature, the bioprocess dynamics is usually modeled by mechanistic models in forms of ordinary/partial differential equations (ODEs/PDEs) (Mandenius et al., 2013). Because they are capable of representing the complex biochemistry of cells in a more complete way (Almquist et al., 2014), mechanistic models become popular and have been widely used in process optimization, design, control, and scale-up (Glen et al., 2018; Liu et al., 2013; Lu et al., 2015; Nfor et al., 2009; Knappert et al., 2020). However, for complex biomanufacturing operations, mechanistic models often oversimplify underlying process mechanisms and make a poor fit to real production data (Teixeira et al., 2007). Thus, domain experts are increasingly adopting data-driven methods for process understanding (Mercier et al., 2013; Kiridar et al., 2007), monitoring (Teixeira et al., 2009), prediction (Gunther et al., 2009), and control (Martagan et al., 2017).

Moreover, those statistical techniques can be used in conjunction with mechanistic models known as hybrid models (Lu et al., 2015; Solle et al., 2017). In comparison to classical approaches, hybrid models usually provide a significantly increased performance, subsequently improving process operation (von Stosch et al., 2014). In recent years, advanced hybrid modeling approaches have been developed and applied to process modeling (von Stosch et al., 2016), optimization (Zhang et al., 2012) and also scale-up (Bollas et al., 2003). Zheng et al. (2021b) proposed a dynamic Bayesian network based hybrid model which can leverage the strengths of both first-principles and data-driven methods. Its applicability to biomanufacturing was investigated by using a yeast cell fermentation. This paper extends such hybrid model to account for nonlinear reactions and bioprocesses with latent state, and further investigates its applicability in cell therapy manufacturing process optimization.

Biomanufacturing Process Optimization: Built on process specifications, classic biomanufacturing optimization and control approaches tend to maintain various process parameters within required ranges in order to guarantee product quality (Jiang and Braatz, 2016) through techniques such as feed-forward, feedback (Hong et al., 2018; Kee et al., 2009; Blanchini et al., 2018), and model predictive control Mesbah et al. (2017); Paulson et al. (2018); Kocijan et al. (2004); Lakerveld et al. (2013). However, the existing strategies derived from PDE/ODE-based deterministic mechanis-

tic models often ignore process inherent stochasticity and model uncertainty.

Reinforcement learning has made many successes in solving some complex problems in healthcare (Zheng et al., 2021a), competitive games (Silver et al., 2016), and other applications. However, these successes are often made in a stationary and well-defined dynamics using a large amount of training samples. In addition, Zheng et al. (2021b) developed a hybrid model based RL framework that builds the process mechanism into a linear Gaussian probabilistic KG, which has been shown to achieve human-level control in low-data environments. However, this method has strong linearity assumption in network structure and fails to take batch-to-batch variation into consideration. To improve the robustness and guarantee the product quality, Pan et al. (2021) proposed a constrained Q-learning algorithm to meet the specification requirements. While there has been some recent work on RL for this domain (Spielberg et al., 2017, 2020; Treloar et al., 2020), these methods often require large training datasets. To improve the sample efficiency, Machalek et al. (2021) proposed a hybrid machine learning physics models based RL approach.

For a highly variable and complex system with limited data, Bayesian reinforcement learning (BRL) has attracted increasing attention due to its advantage in handling model uncertainty (Ghavamzadeh et al., 2016). For example, Mowbray et al. (2021) proposed a data-driven approach that utilizes Gaussian processes for the offline simulation model (a.k.a state transition model) and use the associated posterior uncertainty prediction to account for plant-model mismatch.

3. Problem Statement

In this paper, we model the integrated cell therapy manufacturing process as a finite-horizon Markov decision process (MDP) specified by $(S, \mathcal{A}, H, r, p)$, where S , \mathcal{A} , H , r and p represent state space, action space, planning horizon, deterministic reward function, and state transition probability model. The process state transition, accounting for inherent stochasticity and time-varying dynamics, is modeled as,

$$\mathbf{s}_{t+1} \sim p(\mathbf{s}_{t+1} | \mathbf{s}_t, \mathbf{a}_t; \boldsymbol{\theta}_t) \quad (1)$$

where $\mathbf{s}_t \in S \subset \mathbb{R}^d$ denotes the biomanufacturing process state (e.g., cell density and critical quality attributes (CQAs)), $\mathbf{a}_t \in \mathcal{A}$ is the action (also known as control inputs) at time step t , \mathcal{A} is a finite set of actions with cardinality $|\mathcal{A}|$, and $t \in \mathcal{H} \equiv \{1, 2, \dots, H\}$ denotes the discrete time index (a.k.a. decision epochs). The process dynamics and variations are specified by the model parameters, denoted by $\boldsymbol{\theta} = (\boldsymbol{\theta}_1, \dots, \boldsymbol{\theta}_H)^\top \in \mathbb{R}^{d_\theta}$.

At each time step t , we have the reward function $r_t(\mathbf{s}_t, \mathbf{a}_t)$ and the policy function, mapping the state vector \mathbf{s}_t to an action, i.e., $\mathbf{a}_t = \pi_t(\mathbf{s}_t)$. Thus, the probabilistic model of stochastic decision process (SDP) trajectory $\boldsymbol{\tau} =$

$(\mathbf{s}_1, \mathbf{a}_1, \dots, \mathbf{s}_H, \mathbf{a}_H, \mathbf{s}_{H+1})$ is,

$$p(\boldsymbol{\tau} | \boldsymbol{\theta}) = p(\mathbf{s}_1) \sum_{t=1}^H p(\mathbf{s}_{t+1} | \mathbf{s}_t, \pi_t(\mathbf{s}_t); \boldsymbol{\theta}_t). \quad (2)$$

Given the process model parameters $\boldsymbol{\theta}$, the performance of the policy π is evaluated via the expected accumulated reward,

$$J(\pi; \boldsymbol{\theta}) = \mathbb{E}_{\boldsymbol{\tau}} \left[\sum_{t=1}^{H+1} r_t(\mathbf{s}_t, \mathbf{a}_t) \middle| \pi, \boldsymbol{\theta} \right].$$

In the cell therapy manufacturing, there often exist unobserved state variables (such as cell growth inhibitor, metabolic state), which have substantial impact on the cell production and quality. Let \mathbf{z}_t denote the latent state variable(s). Thus, at any time step t , the process state \mathbf{s}_t includes observable and unobservable (latent) state variables, i.e., $\mathbf{s}_t = (\mathbf{x}_t, \mathbf{z}_t)$ with $\mathbf{x}_t \in S_x$ and latent state variables $\mathbf{z}_t \in S_z$ (represented by gray-shaded node in Figure 1), where $S_x \subset \mathbb{R}^{d_x}$ and $S_z \subset \mathbb{R}^{d_z}$ with $S = S_x \times S_z$ and $d = d_x + d_z$. Therefore, the likelihood of observable trajectory becomes

$$p(\boldsymbol{\tau}_x | \boldsymbol{\theta}) = \int p(\boldsymbol{\tau} | \boldsymbol{\theta}) d\mathbf{z}_1 \cdots d\mathbf{z}_{H+1}$$

where $\boldsymbol{\tau}_x \equiv (\mathbf{x}_1, \mathbf{a}_1, \dots, \mathbf{x}_H, \mathbf{a}_H, \mathbf{x}_{H+1})$ is the trajectory of partially observed state.

The unknown model parameters are estimated with m process observations, denoted by $\mathcal{D} = \{\boldsymbol{\tau}_x^{(i)}; i = 1, \dots, m\}$. In this paper, the model uncertainty is quantified by the posterior distribution by applying Bayesian rule,

$$p(\boldsymbol{\theta} | \mathcal{D}) \propto p(\boldsymbol{\theta}) P(\mathcal{D} | \boldsymbol{\theta}) = p(\boldsymbol{\theta}) \prod_{i=1}^m p(\boldsymbol{\tau}_x^{(i)} | \boldsymbol{\theta})$$

where the prior $p(\boldsymbol{\theta})$ can incorporate the existing knowledge on the model parameters. We will provide the computational Bayesian inference in Section 4.3 to generate B posterior samples quantifying the model uncertainty, i.e., $\boldsymbol{\theta}_b \sim p(\boldsymbol{\theta} | \mathcal{D})$ with $b = 1, 2, \dots, B$.

Thus, we want to find the optimal and robust policy to simultaneously hedge against both inherent stochasticity and model uncertainty, i.e.,

$$\pi^* = \arg \max_{\pi \in \mathcal{P}} J(\pi) \quad (3)$$

where the objective

$$J(\pi) = \mathbb{E}_{\boldsymbol{\theta} \sim p(\boldsymbol{\theta} | \mathcal{D})} [J(\pi; \boldsymbol{\theta})], \quad (4)$$

has inner expectation accounting for stochastic uncertainty and outer expectation accounting for model uncertainty. Since there are often very limited process data in cell therapy manufacturing, the model uncertainty can be large. Ignoring it can lead to unreliable and sub-optimal decision making.

4. Bioprocess Hybrid Modeling and Inference

In this section, we develop a dynamic Bayesian network based hybrid model characterizing the spatial-temporal causal interdependencies of bioprocessing, such as how decision strategies at different times interact with each other and impact on the production process trajectory dynamics. It can leverage on the information from existing mechanistic models and facilitate the learning from process data. The deterministic mechanistic models typically ignore process inherent stochasticity, including batch-to-batch variation, raw material uncertainty, and bioprocess noise, which are often dominant sources of biomanufacturing process variation (Mockus et al., 2015). Thus, we will consider bioprocess noise and raw material uncertainty in Section 4.1, and further extend the hybrid model to incorporate batch-to-batch bioprocess kinetics variation in Section 4.2. The proposed hybrid model can provide the risk- and science-based understanding of integrated biomanufacturing mechanisms. It can improve prediction accuracy and reliability.

Since the state transition probabilistic model for $p(\mathbf{s}_{t+1}|\mathbf{s}_t, \mathbf{a}_t; \boldsymbol{\theta}_t)$ involves latent state variables, nonlinear reactions, and batch-to-batch variation in kinetics, it is challenging to derive the closed form posterior distribution $p(\boldsymbol{\theta}|D)$ quantifying the model uncertainty of integrated bioprocess. Thus, in Section 4.3, we use the approximate Bayesian computation (ABC) approach to generate posterior samples for model inference and facilitate the biomanufacturing mechanisms learning.

4.1. Bioprocess Hybrid Model Development

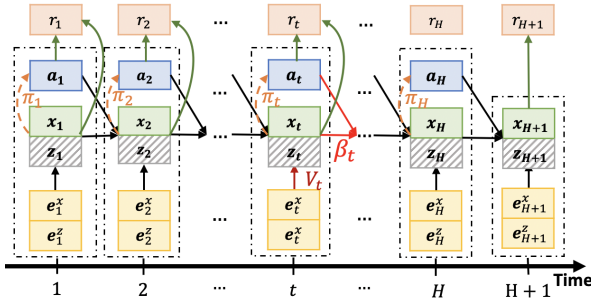


Figure 1: An illustration of policy-augmented knowledge graph (KG) for the stochastic decision process hybrid model.

Given the existing nonlinear ODE-based mechanistic model, denoted by $ds/dt = \mathbf{f}(\mathbf{s}, \mathbf{a}; \boldsymbol{\beta})$, by using the finite difference approximations for derivatives, i.e., $d\mathbf{s} \approx \Delta\mathbf{s}_t = \mathbf{s}_{t+1} - \mathbf{s}_t$, and $dt \approx \Delta t$, we construct the hybrid model for state transition,

$$\mathbf{x}_{t+1} = \mathbf{x}_t + \Delta t \cdot \mathbf{f}_x(\mathbf{x}_t, \mathbf{z}_t, \mathbf{a}_t; \boldsymbol{\beta}_t) + \mathbf{e}_{t+1}^x, \quad (5)$$

$$\mathbf{z}_{t+1} = \mathbf{z}_t + \Delta t \cdot \mathbf{f}_z(\mathbf{x}_t, \mathbf{z}_t, \mathbf{a}_t; \boldsymbol{\beta}_t) + \mathbf{e}_{t+1}^z, \quad (6)$$

with unknown d_β -dimensional kinetic coefficients $\boldsymbol{\beta}_t \in \mathbb{R}^{d_\beta}$ (e.g., cell growth rate, inhibition effect). The residual terms are modeled by multivariate Gaussian distribution $\mathbf{e}_{t+1}^x \sim$

$\mathcal{N}(0, V_{t+1}^x)$ and $\mathbf{e}_{t+1}^z \sim \mathcal{N}(0, V_{t+1}^z)$ with zero means and covariance matrices V_{t+1}^x and V_{t+1}^z . The kinetic coefficients $\boldsymbol{\beta}_t$ can change over different phases of cell culture (e.g., growth and stationary phases) to represent the fact that the bioprocess dynamics is time-varying. By abuse of notation, we use the subscript t to represent time index in the proposed model. For notation simplification, we consider fixed time step Δt even through the proposed methodology can be applicable to general situations with heterogenous process data.

The statistical residual terms $\mathbf{e}_t = (\mathbf{e}_t^x, \mathbf{e}_t^z)$ allow us to account for the impact from bioprocess noise, raw material uncertainty, uncontrolled critical process parameters (CPPs), and other uncontrollable factors (e.g., contamination) occurring at any time step t . They can facilitate the learning such as identifying ignored CPPs.

Let $\mathbf{g}_x(\mathbf{x}_t, \mathbf{z}_t, \mathbf{a}_t; \boldsymbol{\beta}_t) \equiv \mathbf{x}_t + \Delta t \cdot \mathbf{f}_x(\mathbf{x}_t, \mathbf{z}_t, \mathbf{a}_t; \boldsymbol{\beta}_t)$ and $\mathbf{g}_z(\mathbf{x}_t, \mathbf{z}_t, \mathbf{a}_t; \boldsymbol{\beta}_t) \equiv \mathbf{z}_t + \Delta t \cdot \mathbf{f}_z(\mathbf{x}_t, \mathbf{z}_t, \mathbf{a}_t; \boldsymbol{\beta}_t)$. Equivalently, we can rewrite the state transition model (5) and (6) as,

$$\mathbf{x}_{t+1}|\mathbf{x}_t, \mathbf{z}_t, \mathbf{a}_t \sim \mathcal{N}(\mathbf{g}_x(\mathbf{x}_t, \mathbf{z}_t, \mathbf{a}_t; \boldsymbol{\beta}_t), V_{t+1}^x), \quad (7)$$

$$\mathbf{z}_{t+1}|\mathbf{x}_t, \mathbf{z}_t, \mathbf{a}_t \sim \mathcal{N}(\mathbf{g}_z(\mathbf{x}_t, \mathbf{z}_t, \mathbf{a}_t; \boldsymbol{\beta}_t), V_{t+1}^z). \quad (8)$$

Let the state transition model parameters $\boldsymbol{\theta}_t$ representing the composite parameters including kinetic coefficients and the variances of process residuals, i.e., $\boldsymbol{\theta}_t = (\boldsymbol{\beta}_t, \text{vec}(V_{t+1}^x), \text{vec}(V_{t+1}^z))^\top$. We use $\text{vec}(\cdot)$ to denote a linear transformation converting an $n \times m$ matrix into a $nm \times 1$ column vector. Let $g(\mathbf{s}_t, \mathbf{a}_t; \boldsymbol{\beta}_t) \equiv \mathbf{s}_t + \Delta t \cdot \mathbf{f}(\mathbf{s}_t, \mathbf{a}_t; \boldsymbol{\beta}_t)$. Then, at any time step $t \in \mathcal{H}$, we have the full state transition

$$\begin{aligned} \mathbf{s}_{t+1}|\mathbf{s}_t, \mathbf{a}_t &= g(\mathbf{s}_t, \mathbf{a}_t; \boldsymbol{\beta}_t) + \mathbf{e}_{t+1} \\ &\sim \mathcal{N}(g(\mathbf{s}_t, \mathbf{a}_t; \boldsymbol{\beta}_t), V_{t+1}) \end{aligned} \quad (9)$$

where $\mathbf{s}_t = (\mathbf{x}_t, \mathbf{z}_t)$, $\mathbf{e}_{t+1} = (\mathbf{e}_{t+1}^x, \mathbf{e}_{t+1}^z)$ and V_{t+1} is diagonal covariance matrix with diagonal entries from V_{t+1}^x and V_{t+1}^z .

The stochastic decision process (SDP) of integrated biomanufacturing system can be visualized by the probabilistic directed network as shown in Figure 1. This network models the causal effects (with directed edges representing causal interactions) of current state and action $\{\mathbf{s}_t, \mathbf{a}_t\}$ on future states $\mathbf{s}_{t'}$ with $t' > t$ through mechanism pathways; see eq. (9). The observed state \mathbf{x}_t and latent state \mathbf{z}_t are represented by solid and shaded nodes respectively. With the introduction of decision policies, we create a *policy augmented KG* by including additional edges: 1) connecting state \mathbf{s}_t to action \mathbf{a}_t representing the causal effect of the policy, $\mathbf{a}_t = \pi_t(\mathbf{s}_t)$; and 2) connecting actions and states to reward $r_t(\mathbf{s}_t, \mathbf{a}_t)$ (i.e., cost, cell product productivity).

In this paper, we consider the case studies with prior knowledge on the underlying bioprocess mechanisms — the form of function $\mathbf{f}(\cdot)$ is known but the coefficients $\boldsymbol{\beta}$ are unknown. In the situations without any strong prior knowledge on the underlying bioprocess mechanisms (i.e., $\mathbf{f}(\cdot)$ is unknown) or the cases with intensive online monitoring (i.e.,

Δt is small), we can use a linear statistical function modeling the state transition to consider the main effects. Specifically, at any time step $t \in \mathcal{H}$, we model the state transition as $\mathbf{s}_{t+1} = \boldsymbol{\beta}_t^s \mathbf{s}_t + \boldsymbol{\beta}_t^a \mathbf{a}_t + \mathbf{e}_{t+1}$, where the coefficients $\boldsymbol{\beta}_t^s$ and $\boldsymbol{\beta}_t^a$ measure the main effects of current state \mathbf{s}_t and action \mathbf{a}_t on next state \mathbf{s}_{t+1} , and \mathbf{e}_{t+1} represents the residual. We refer to Zheng et al. (2021b); Xie et al. (2020) for more details about linear Gaussian Bayesian network based hybrid model.

4.2. Batch-to-Batch Variation Modeling

To further account for batch-to-batch variation, the kinetic coefficients are modeled by random variables,

$$\boldsymbol{\beta}_t = \boldsymbol{\mu}_t^\beta + \boldsymbol{\epsilon}_t^\beta \quad (10)$$

where $\boldsymbol{\epsilon}_t^\beta$ represents the random batch effect following a multivariate normal distribution with mean zero and covariance matrix Σ_β . The vector $\boldsymbol{\mu}_t^\beta$ represents the mean of kinetic coefficients. Then, the state transition in (5) and (6) becomes

$$\mathbf{x}_{t+1} = \mathbf{g}_x(\mathbf{x}_t, \mathbf{z}_t, \mathbf{a}_t, \boldsymbol{\beta}_t; \boldsymbol{\theta}_t) + \mathbf{e}_{t+1}^x, \quad (11)$$

$$\mathbf{z}_{t+1} = \mathbf{g}_z(\mathbf{x}_t, \mathbf{z}_t, \mathbf{a}_t, \boldsymbol{\beta}_t; \boldsymbol{\theta}_t) + \mathbf{e}_{t+1}^z, \quad (12)$$

where $\boldsymbol{\beta}_t \sim \mathcal{N}(\boldsymbol{\mu}_t^\beta, \Sigma_\beta)$, $\mathbf{e}_{t+1}^x \sim \mathcal{N}(0, V_{t+1}^x)$, and $\mathbf{e}_{t+1}^z \sim \mathcal{N}(0, V_{t+1}^z)$, representing inherent stochasticity. Thus, the biomanufacturing SDP hybrid model is specified by the parameters, $\boldsymbol{\theta}_t = (\boldsymbol{\mu}_t^\beta, \text{vec}(\Sigma_\beta), \text{vec}(V_{t+1}^x), \text{vec}(V_{t+1}^z))^\top$.

4.3. Process Model Uncertainty Quantification

Given the biomanufacturing process realizations $\mathcal{D} = \{\boldsymbol{\tau}_x^{(i)}; i = 1, \dots, m\}$, the ABC sampling approach (Minter and Retkute, 2019; Toni et al., 2009; McKinley et al., 2018; Beaumont et al., 2009) is used to generate B posterior samples of model parameters from the posterior distribution $p(\boldsymbol{\theta}|\mathcal{D})$ quantifying the model estimation uncertainty. For any i -th process trajectory observation $\boldsymbol{\tau}_x^{(i)}$, the algorithm jointly simulates the parameters of the hybrid model $\boldsymbol{\theta} \sim p(\boldsymbol{\theta})$ and predicted trajectories $\boldsymbol{\tau}_x^{*(ij)} \sim p(\boldsymbol{\tau}_x|\boldsymbol{\theta})$ for $j = 1, 2, \dots, L$. We accept the samples of parameters (called particles) with the tolerance of the averaged discrepancy or distance between the real process observations and simulated data. We define the distance as,

$$q \equiv \frac{1}{mL} \sum_{i=1}^m \sum_{j=1}^L d(\boldsymbol{\tau}_x^{(i)}, \boldsymbol{\tau}_x^{*(ij)}),$$

where $d(\cdot, \cdot)$ is the distance function, $\boldsymbol{\tau}_x^{*(ij)}$ is the predicted partially observed process trajectory and $\delta > 0$ is the tolerance bound. In this paper, we use the square root of the sum of squared differences between trajectories as the distance measure, i.e., $d(\mathbf{x}, \mathbf{y}) \equiv \|\mathbf{x} - \mathbf{y}\|$ for any \mathbf{x} and \mathbf{y} . For any d -dimensional vector $\mathbf{x} \in \mathbb{R}^d$, we consider L2 norm $\|\mathbf{x}\| \triangleq \|\mathbf{x}\|_2 = \sqrt{\sum_{i=1}^d x_i^2}$. Thus, through gradually reducing the tolerance level δ , we better approximate the posterior distribution $p(\boldsymbol{\theta}|\mathcal{D})$ using those selected samples of $\boldsymbol{\theta}$,

$$p(\boldsymbol{\theta}|\mathcal{D}) \approx p(\boldsymbol{\theta}|q \leq \delta). \quad (13)$$

We use the sequential Monte Carlo (SMC) to efficiently explore the parameter space and generate posterior samples. Specifically, in ABC-SMC, a number of accepted posterior samples, $\{\boldsymbol{\theta}_1, \dots, \boldsymbol{\theta}_B\}$, sampled from the prior distribution $p(\boldsymbol{\theta})$, are propagated through a sequence of intermediate distributions, $p(\boldsymbol{\theta}|q \leq \delta_g)$ for $g = 1, \dots, G$, until it represents the samples from the target distribution $p(\boldsymbol{\theta}|q \leq \delta_G)$. The tolerance bounds δ_g are chosen such that $\delta_1 > \delta_2 > \dots > \delta_G$ and the distributions gradually evolve towards the target posterior $p(\boldsymbol{\theta}|\mathcal{D})$. The approximation quality increases as δ_g decreases with iteration g . We use the adaptive scheme introduced in Lenormand et al. (2013) to select the decreasing sequence of tolerance levels.

The pseudocode is provided at Algorithm 1. The initial set of posterior samples $\{\boldsymbol{\theta}_b^{(0)}\}_{b=1}^N$ is generated from the prior distribution $p(\boldsymbol{\theta})$. The associated weights $\{w_b^{(0)}\}_{b=1}^N$ and distances $\{q_b^{(0)}\}_{b=1}^N$ are calculated in **Steps 2-3**. For each i -th observation, we generate L predicted trajectories and calculate the distance $q_b^{(0)}$. The next tolerance level δ_1 is determined online as the first α -quantile of the $\{q_b^{(0)}\}_{b=1}^N$ (**Step 4**). The updated posterior distribution approximation, specified by $\{\boldsymbol{\theta}_b, w_b, q_b\}_{b=1}^B$ with $B = \lfloor \alpha N \rfloor$, is then constituted from the particles satisfying the tolerance level δ_1 (**Step 5**), with $N - B$ new particles drawn from weighted sample set $\{\boldsymbol{\theta}_k^{g-1}\}_{k=1}^B$ and perturbed by kernel K (**Steps 6-7**). Similar to **Step 1** to **5**, the associated weights and distances are calculated (**Steps 8-10**), the next tolerance level δ_g and posterior approximation are updated (**Steps 12-13**). The algorithm stops when the proportion p_{acc} of particles satisfying the tolerance level δ_{g-1} among the $N - B$ new particles is below the threshold $p_{acc, min}$ (**Step 11**). We refer to Lenormand et al. (2013) for more details.

5. Model-based Reinforcement Learning

We formulate the biomanufacturing process optimization and control as a finite-horizon MDP. The process starts with an initial state \mathbf{s}_1 . At any time step t , the agent observes the state \mathbf{s}_t , chooses an action \mathbf{a}_t , and receives a reward $r_t = r_t(\mathbf{s}_t, \mathbf{a}_t)$. Then the process transits to a new state \mathbf{s}_{t+1} at next time step $t + 1$ by following the state transition distribution $p(\mathbf{s}_{t+1}|\mathbf{s}_t, \mathbf{a}_t, \boldsymbol{\theta}_t)$. The episode terminates when \mathbf{s}_{H+1} is reached and the agent takes the ‘‘Harvest’’ action. Since there are often very limited process observations in cell therapy manufacturing, the goal is to *sample efficiently* learn an optimal policy (3) by maximizing the expected total reward (4) accounting for model uncertainty.

For each $t \in \mathcal{H}$, we define the value function $V_t^\pi(\mathbf{s}) : \mathcal{S} \rightarrow \mathbb{R}$ as the expected value of cumulative rewards received under policy π when starting from state \mathbf{s} at the t -th step, i.e.,

$$V_t^\pi(\mathbf{s}) = \mathbb{E}_{p(\boldsymbol{\theta}|\mathcal{D})} \mathbb{E}_{p(\mathbf{s}_{t+1}|\mathbf{s}_t, \pi_t(\mathbf{s}_t), \boldsymbol{\theta}_t)} \left[\sum_{\ell=t}^H r_\ell(\mathbf{s}_\ell, \pi_\ell(\mathbf{s}_\ell)) \mid \mathbf{s}_t = \mathbf{s} \right]$$

where the outer expectation $\mathbb{E}_{p(\boldsymbol{\theta}|\mathcal{D})}[\cdot]$ accounts for model uncertainty. Given a posterior sample of model parameters

Algorithm 1: Adaptive Population Monte Carlo ABC (Lenormand et al., 2013)

Input: $p(\theta)$, the prior distribution of θ ; N , the number of particles; $\{\tau_x^{(i)}\}_{i=1}^m$, m partially observed bioprocess trajectories; K , the perturbation Kernel; α , the ratio of particles to keep at each iteration ($\alpha \in [0, 1]$), and $p_{acc, min}$, the minimal acceptance rate.

Output: ABC posterior distribution samples with corresponding weight and distance $\{\theta_b, w_b, q_b\}_{b=1}^B$, where $B = \lfloor \alpha N \rfloor$.

for $b = 1, \dots, N$ **do**

1. Sample $\theta_b^{(0)}$ from the prior distribution $p(\theta)$;
2. Generate L predicted trajectories $\{\tau_x^{*(ij)}\}_{j=1}^L$ using $\theta_b^{(0)}$, with $i = 1, \dots, m$;
3. Set $q_b^{(0)} = \frac{1}{mL} \sum_{i=1}^m \sum_{j=1}^L d(\tau_x^{(i)}, \tau_x^{*(ij)})$ and $w_b^{(0)} = 1$;

4. Let δ_1 be the first α -quantile of $q^{(0)} = \{q_b^{(0)}\}_{b=1}^N$;

5. Let $\{(\theta_b^{(1)}, w_b^{(1)}, q_b^{(1)})\} = \{(\theta_b^{(0)}, w_b^{(0)}, q_b^{(0)}) | q_b^{(0)} \leq \delta_1, 1 \leq b \leq N\}$, $p_{acc} = 1$ and $g = 2$;

while $p_{acc} > p_{acc, min}$ **do**

for $b = B + 1, \dots, N$ **do**

6. Sample θ_b^* from $\theta_k^{(g-1)}$ with probability $\frac{w_k^{(g-1)}}{\sum_{j=1}^B w_j^{(g-1)}}$, $1 \leq k \leq B$;
7. Perturb the particle to obtain $\theta_b^{(g-1)} \sim K(\theta | \theta_b^*) = \mathcal{N}(\theta_b^*, \Sigma)$;
8. Generate L predicted trajectories $\{\tau_x^{*(ij)}\}_{j=1}^L$ using $\theta_b^{(g-1)}$, with $i = 1, \dots, m$;
9. Set $q_b^{(g-1)} = \frac{1}{mL} \sum_{i=1}^m \sum_{j=1}^L d(\tau_x^{(i)}, \tau_x^{*(ij)})$;
10. Set $w_b^{(g-1)} = \frac{p(\theta_b^{(g-1)})}{\sum_{j=1}^B \frac{w_j^{(g-1)}}{\sum_{k=1}^B w_k^{(g-1)}} K(\theta_b^{(g-1)} | \theta_j^{(g-1)})}$;

11. Set $p_{acc} = \frac{1}{N-B} \sum_{k=B+1}^N \mathbb{1}(q_k^{(g-1)} \leq \delta_{g-1})$;

12. Let δ_g be the first α -quantile of $q^{(g-1)} = \{q_b^{(g-1)}\}_{b=1}^N$;

13. Let $\{(\theta_b^{(g)}, w_b^{(g)}, q_b^{(g)})\} = \{(\theta_b^{(g-1)}, w_b^{(g-1)}, q_b^{(g-1)}) | q_b^{(g-1)} \leq \delta_g, 1 \leq b \leq N\}$ and $g = g + 1$;

$\theta \sim p(\theta | \mathcal{D})$, the inner expectation $\mathbb{E}_{p(s_{t+1} | s_t, \pi(s_t), \theta_t)}[\cdot]$ is taken over the state transition model (11) and (12) under the policy function π . Accordingly, we also define the action-value Q-function, denoted by $Q_t^\pi : S \times \mathcal{A} \rightarrow \mathbb{R}$, which gives the expected value of cumulative rewards when the agent starts from an arbitrary state-action pair, say $(s, a) \in S \times \mathcal{A}$, at the t -th step and follows policy π afterwards, i.e.,

$$Q_t^\pi(s, a) = \mathbb{E} \left[\sum_{\ell=t}^H r_\ell(s_\ell, \pi_\ell(s_\ell)) \mid s_t = s, a_t = a \right]$$

$$= r_t(s, a) + \mathbb{E} \left[V_{t+1}^\pi(s_{t+1}) \mid s_t = s, a_t = a \right] \quad (14)$$

where the expectation is taken over both posterior distribution $p(\theta | \mathcal{D})$ and the transition distribution $p(s_{t+1} | s_t, a_t, \theta_t)$ for all $t \in T$ by following the policy $a_t = \pi(s_t)$. For notation simplification, we use $\mathbb{E}[\cdot] = \mathbb{E}_{p(\theta | \mathcal{D})} \mathbb{E}_{p(s_{t+1} | s_t, \pi(s_t), \theta_t)}[\cdot]$ in the following discussion if not mentioned otherwise.

Here we consider a greedy policy (Puterman, 2014), i.e.,

$$\pi_t(s) \equiv \arg \max_{a \in \mathcal{A}} Q_t(s, a), \text{ for any } s \in S. \quad (15)$$

It is known that the optimal policy π is the greedy policy with respect to the optimal action-value function and thus it suffices to estimate the optimal action-value functions (Jin et al., 2020). Then we can rewrite (14) as

$$Q_t(s, a) = r_t(s, a) + \mathbb{E} \left[\max_{a \in \mathcal{A}} Q_{t+1}(s_{t+1}, a_{t+1}) \mid s_t = s, a_t = a \right]. \quad (16)$$

The sampling procedure of hybrid model-based Bayesian RL for process optimization is summarized in Algorithm 2. The goal of process optimization is to find the optimal action at each time step which maximizes the expected total rewards. To solve the problem, we propose a solution approach which estimates Q-value (16) from starting time t to the planning horizon (**Step 1**) and then selects the optimal action by using the greedy policy (**Step 2**). After that, we execute the action and observe the next state (**Step 3**).

Algorithm 2: Hybrid model-based Bayesian RL Sampling Procedure for Process Optimization.

Input: The initial state s_1

Output: Optimal actions a_t^* for $t = 1, 2, \dots, H$

for $t = 1, 2, \dots, H$ **do**

for $a_t \in \mathcal{A}$ **do**

1. $q_t(a_t) = \text{QFUN}(t, s_t, a_t)$ (Algorithm 3);

2. Find the greedy optimal action (15):

$a_t^* = \arg \max_{a_t \in \mathcal{A}} q_t(a_t)$;

3. Apply the optimal action and evolve to next state, i.e., $s_{t+1} = \mathbb{E}_{p(\theta_t | \mathcal{D})} [\mathbb{E}[s_{t+1} | s_t, a_t^*, \theta_t]]$.

We estimate the Q-function $Q_t(s, a)$ by simulating the bioprocess hybrid model and applying the sparse sampling method (Wang et al., 2021a; Kearns et al., 2002; Wang et al., 2005). Specifically, we generate future trajectories accounting for both bioprocess inherent stochasticity and model uncertainty. Then, we search for the optimal action through look-ahead tree. Bayesian sparse sampling grows a look-ahead tree starting with the root at the current state, enumerating actions at decision nodes, and sampling at outcome nodes over both posterior distribution and state transition distribution. The same procedure is repeated for each node until all the leaf nodes reach the end of the planning horizon.

Algorithm 3: Bayesian Sparse Sampling for Estimating Q Function and Value Function

Input: Current state \mathbf{s}_t . Obtain a set of posterior samples $\Theta = \{\boldsymbol{\theta}_b\}_{b=1}^B$ with their associated weights $\{w_b\}_{b=1}^B$, the number of posterior samples B , and the number of samples from state transition distribution N from Algorithm 1.

Output: Estimated the value of Q-function $\hat{Q}(\mathbf{s}, \mathbf{a})$

Function QFUN($t, \mathbf{s}_t, \mathbf{a}_t$):

```

for  $b = 1, 2, \dots, B$  do
  (A1) Sample  $\boldsymbol{\theta}_b$  from weighted posterior
        distribution  $\Theta$  (Equivalently  $\boldsymbol{\theta}^b \sim p(\boldsymbol{\theta}_t | \mathcal{D})$ ).
  for  $j = 1, \dots, N$  do
    (A2) Sample from state transition
          distribution  $\mathbf{s}_{t+1}^{(b,j)} \sim p(\mathbf{s}_{t+1} | \mathbf{s}_t, \mathbf{a}_t, \boldsymbol{\theta}_{t,b})$ 
    (A3)  $V_{t+1}(\mathbf{s}_{t+1}^{(b,j)}) = \text{VFUN}(t, \mathbf{s}_{t+1}^{(b,j)})$ 
  (A4)  $\hat{Q}_t(\mathbf{s}_t, \mathbf{a}_t) =$ 
       $r_t(\mathbf{s}_t, \mathbf{a}_t) + \frac{1}{BN} \sum_{b=1}^B \sum_{j=1}^N V_{t+1}(\mathbf{s}_{t+1}^{(b,j)})$ .
return  $\hat{Q}_t(\mathbf{s}_t, \mathbf{a}_t)$ .

```

End Function

Function VFUN(t, \mathbf{s}_t):

```

if  $t = H + 1$  then
  return  $r_{H+1}(\mathbf{s}_{H+1}, \mathbf{a}_{H+1} = \text{"Harvest"})$ ;
for  $\mathbf{a}_t \in \mathcal{A}$  do
  for  $b = 1, 2, \dots, B$  do
    (B1) Sample from weighted posterior
          distribution  $\boldsymbol{\theta}_b \sim p(\boldsymbol{\theta}_t | \mathcal{D})$ 
    for  $j = 1, \dots, N$  do
      (B2) Sample from state transition
             $\mathbf{s}_{t+1}^{(b,j)} \sim p(\mathbf{s}_{t+1} | \mathbf{s}_t, \mathbf{a}_t, \boldsymbol{\theta}_{t,b})$ 
      (B3)  $V_{t+1}(\mathbf{s}_{t+1}^{(b,j)}) = \text{VFUN}(t, \mathbf{s}_{t+1}^{(b,j)})$ 
    (B4) Estimate  $\hat{Q}_t(\mathbf{s}_t, \mathbf{a}_t) =$ 
       $r_t(\mathbf{s}_t, \mathbf{a}_t) + \frac{1}{BN} \sum_{b=1}^B \sum_{j=1}^N V_{t+1}(\mathbf{s}_{t+1}^{(b,j)})$ 
    (B5)  $\hat{V}_t(\mathbf{s}_t) = \max_{\mathbf{a}_t \in \mathcal{A}} \hat{Q}_t(\mathbf{s}_t, \mathbf{a}_t)$ 

```

End Function

The procedure of Bayesian sparse sampling for Q-function and the value function estimation is summarized in Algorithm 3. The Q-function (and the value function) estimates are computed from leaf nodes rolling-backing up to the root. To compute the value function VFUN(t, \mathbf{s}_t), we grow a look-ahead tree starting with the root at the current state. For each action $\mathbf{a} \in \mathcal{A}$, we grow the root into BN child nodes with each representing a sample of the next state, i.e., $(\mathbf{s}_{t+1}^{(b,j)})$ from state transition probability $p(\mathbf{s}_{t+1} | \mathbf{s}_t, \mathbf{a}_t, \boldsymbol{\theta}_{t,b})$, where the posterior samples $\boldsymbol{\theta}_{t,b} \sim p(\boldsymbol{\theta} | \mathcal{D})$ with $b = 1, \dots, B$ are generated with ABC-SMC and we create N trajectories at each model posterior sample (Step B1-B3). The same procedure is repeated for each node until all the leaf nodes

reach the end of the process, e.g., the ‘‘Harvest’’ decision is made at $H + 1$ time step. Then the expected Q-value in (14) is obtained by the sum of an immediate reward $r_t(\mathbf{s}_t, \mathbf{a}_t)$ and the expected value $\mathbb{E} \left[V_{t+1}^\pi(\mathbf{s}_{t+1}) \mid \mathbf{s}_t, \mathbf{a}_t \right]$ estimated by sample average approximation (Step B4). The value of current state and optimal action are obtained by maximizing the Q values (Step B5-B6). The Q-value function ‘‘QFUN’’ is calculated in a similar way as ‘‘VFUN’’. The only difference is that the current action \mathbf{a}_t is given as the input of QFUN so that we remove the step of enumerating all candidate actions at time step t and then return $\hat{Q}_t(\mathbf{s}_t, \mathbf{a}_t)$ calculated in (B4).

Then, the Q-value estimate QFUN($t, \mathbf{s}_t, \mathbf{a}_t$) is used for process control. In the process optimization problem, giving an initial state \mathbf{s}_1 , the RL agent interacts with estimated dynamics $p(\mathbf{s}_{t+1} | \mathbf{s}_t, \mathbf{a}_t) = \mathbb{E}_{p(\boldsymbol{\theta}_t | \mathcal{D})} [p(\mathbf{s}_{t+1} | \mathbf{s}_t, \mathbf{a}_t, \boldsymbol{\theta}_t)]$ and makes the action maximizing the Q-value according to the greedy policy (15). In the process control, we execute the greedy policy in an online manner, which means that we focus on estimating the Q-function in (16) at a particular current state $(\mathbf{s}_t, \mathbf{a}_t)$ and take the action which has the greatest estimated Q values. After the action is executed, we move to the next decision epoch with a new observed state at which the entire procedure is repeated.

6. Cell Therapy Manufacturing Case Study

In this section, we use the erythroblast cell therapy manufacturing example presented in Glen et al. (2018) to assess the performance of proposed hybrid model-based RL. The cell culture of erythroblast exhibits two phases: a relatively uninhibited growth followed by an inhibited phase. Glen et al. (2018) identified that this reversible inhibition is caused by a unknown cell-driven factor rather than commonly known mass transfer or metabolic limitations.

6.1. Cell Culture Process Hybrid Modeling

Glen et al. (2018) developed an ODE-based mechanistic model describing the dynamics of an unidentified autocrine growth inhibitor accumulation and its impact on the erythroblast cell production process. We extend this model to a two-phase cell culture process, including growth and stationary phases, represented by the phase index $p \in \{\text{‘‘growth’’}, \text{‘‘stationary’’}\}$. The mechanistic model of cell growth and inhibitor accumulation for the p -th phase is

$$\frac{d\rho}{dt} = r_p^g \rho \left(1 - \left(1 + e^{(k_p^s (k_p^c - I))} \right)^{-1} \right), \quad (17)$$

$$\frac{dI}{dt} = \frac{d\rho}{dt} - r_p^d I, \quad (18)$$

where ρ_t and I_t represent the cell density and the inhibitor concentration at time t . The kinetic coefficients r_p^g , k_p^s , k_p^c and r_p^d denote the cell growth rate, inhibitor sensitivity, inhibitor threshold, and inhibitor decay. Suppose that the phase transition occurs at $T_\star = 18$ hour.

Given the mechanistic model in eq. (17)–(18), by following the presentation in Section 4.1, we construct the hybrid

model,

$$\rho_{t+1} = \rho_t + \Delta t \cdot r_t^g \rho_t \left(1 - \left(1 + e^{(k_t^s(k_t^c - I))} \right)^{-1} \right) + e_t^\rho,$$

$$I_{t+1} = I_t + \Delta t \cdot \left(\frac{\rho_{t+1} - \rho_t}{\Delta t} - r_t^d I_t \right) + e_t^I,$$

where the residuals follow the normal distributions $e_t^\rho \sim \mathcal{N}(0, (v_t^\rho)^2)$ and $e_t^I \sim \mathcal{N}(0, (v_t^I)^2)$.

A set of historical data of erythroblast growth from four different donors was analysed by Glen et al. (2018) to provide the insight into autologous variation. Their investigation shows that only the growth rate has significant variability. In order to accommodate the batch-to-batch variation, we model the growth rate as normally distributed random variable $r_t^g \sim \mathcal{N}(\mu_t^g, (\sigma_t^g)^2)$. Thus, the collection of hybrid model parameters is $\theta_t = [\mu_t^g, \sigma_t^g, k_t^s, k_t^c, r_t^d, v_t^\rho, v_t^I]$. For the two-phase cell culture process, we consider different sets of parameter values for the growth and stationary phases.

6.2. Simulation Data Generation

To assess the performance of proposed hybrid model and model-based RL framework, we create the simulation model capturing the key sources of uncertainty. It works as a ground-truth model to generate “real data” to validate the performance of proposed hybrid-RL framework. Based on the ICH Q11 regulatory guidance on drug substance manufacture and quality (McDonald and Ho, 2012), “identification of potential sources of process variability” is listed as a key aspect of quality-by-design (QbD). Hence the modeling of different source process variation plays an important role in the model quality improvement and reliability of process optimization. To faithfully represent the real system, we incorporate four sources of uncertainty into the deterministic mechanistic model (17)–(18), including the variation in initial cell density, measurement error, batch-to-batch variation, and bioprocess noise.

The ground-truth cell culture process is modeled as stochastic differential equations,

$$d\rho = r_p^g \rho \left(1 - \left(1 + e^{(k^s(k^c - I))} \right)^{-1} \right) dt + \sigma_n dW \quad (19)$$

$$dI = d\rho - r^d I dt + \sigma_n dW \quad (20)$$

with random initial values (boundary conditions)

$$\rho_0 \sim \mathcal{N}(\mu_\rho, \sigma_\rho^2) \quad \text{and} \quad I_0 = 0$$

where $r_p^g \sim \mathcal{N}(\mu_p^g, (\sigma_p^g)^2)$ with $p \in \{\text{“growth”}, \text{“stationary”}\}$. In the computer simulation, the above stochastic differential equations (SDE) can be computed by discretizing the Wiener process with a timestep dt as $dW \approx \sqrt{dt} \mathcal{N}(0, 1)$ (Bayram et al., 2018; Malham and Wiese, 2010). At any measurement time step $t \in \mathcal{H}$, we add measurement error to the measured cell density by $\rho_t \leftarrow \rho_t + e_m$ with the measurement error following a normal distribution $e_m \sim \mathcal{N}(0, \sigma_m^2)$.

The variance in initial cell density may come from inadequate mixing, inoculum size, processing time, and storage time (Rain-Franco et al., 2021). The bioprocess noise term $\sigma_n dW$ represents the microbial cell-to-cell phenotypic diversity (Vasdekis et al., 2015). We further incorporate batch-to-batch variation by considering the random effect on the growth rate. In specific, we model the random influence incurred by batch-to-batch variation by $r_p^g = \mu_p^g + e_p^g$, where μ_p^g represents the mean of growth rate and the random effect e_p^g is modeled as a normal distribution with mean zero and standard deviation σ_p^g . Note that the above model allows for batch-to-batch variation to affect each j -th simulated trajectory by realizing $r_j^g \sim \mathcal{N}(\mu_p^g, (\sigma_p^g)^2)$ for $j = 1, 2, \dots, n$.

6.3. Process Model Inference and Validation

In the case study, we set the initial state of cell density $\rho_0 \sim \mathcal{N}(3, 0.03^2)$ and the measurement uncertainty $\sigma_m = 0.2$. By using the synthetic data generated from the “ground-truth” simulation model (19)–(20) in Section 6.2, we compare the performance of the proposed SDP hybrid model with the deterministic mechanistic model estimated by using least square method (LS) under the situations with different levels of bioprocess inherent stochasticity and model uncertainty (i.e., the scenarios with different sizes of real-world observations $m = 3, 6, 20$ batches). For stochastic uncertainty, we are interested in the effect of batch-to-batch variation and bioprocess noise. We set the high and low batch-to-batch variation $\sigma_p^g = 0.016, 0.008$ for both phases, and set high and low bioprocess noise $\sigma_n = 0.03, 0.01$. The means of cell growth rates r_p^g are fixed as $\mu_{growth}^g = 0.057$ at growth phase and $\mu_{stationary}^g = 0.0285$ at stationary phase. Other bioprocess parameters are set as $\{k^s, k^c, r^d\} = \{3.4, 2.6, 0.005\}$ for both phases.

We utilize the ABC sampling approach presented in Section 4.3 to generate posterior samples of bioprocess model parameters. Let the number of particles $N = 200$, the ratio $\alpha = 0.5$, the number of replications $L = 20$, and the minimal accept rate $P_{accmin} = 0.05$. The prior distributions of hybrid model parameters are set as: $\mu_p^g \sim U(0, 0.2)$, $\sigma_t^g \sim U(0, 0.05)$, $k_p^s \sim U(0, 5)$, $k_p^c \sim U(0, 5)$, $r_p^d \sim U(0, 0.05)$, $e_p^\rho \sim U(0, 0.2)$ and $e_p^I \sim U(0, 0.2)$ for $p \in \{\text{“growth”}, \text{“stationary”}\}$.

We conduct simulation experiments to assess the prediction performance of the hybrid model estimated by Bayesian inference and the ODE-based mechanistic model with the LS estimates. The error at each t -th time step is defined as

$$E_s(t, r) = \frac{1}{N} \sum_{i=1}^N \text{Err}_s(t, f_r)$$

where $\{s_{[1:H]}^{(i)}\}_{i=1}^N$ are N test bioprocess trajectories sampled from “ground-truth” simulator, $\text{Err}_s(t, f_r) = |s_t^{(i)} - \hat{s}_t|$, $s \in \{\rho, I\}$ and $f_r \in \{\text{“hybrid”}, \text{“LS”}\}$ represents the model (fitted by random trajectory samples ($m = 3, 6, 20$) through our model and least square model in r -th macro-replication).

Table 1

The prediction error (MAE) of expected erythroblast cell density of hybrid model and LS.

Noise Level		Time (hrs)	Hybrid			LS		
b2b variation	process noise		$m = 3$	$m = 6$	$m = 20$	$m = 3$	$m = 6$	$m = 20$
high	$\sigma_n = 0.01$	3	0.12 ± 0.05	0.09 ± 0.03	0.06 ± 0.02	0.41 ± 0.19	0.59 ± 0.30	0.44 ± 0.22
		18	0.60 ± 0.17	0.48 ± 0.10	0.26 ± 0.07	0.74 ± 0.15	0.57 ± 0.25	0.49 ± 0.23
		30	0.59 ± 0.16	0.40 ± 0.11	0.22 ± 0.06	0.65 ± 0.24	0.70 ± 0.36	0.84 ± 0.65
high	$\sigma_n = 0.03$	3	0.21 ± 0.05	0.14 ± 0.03	0.08 ± 0.03	0.37 ± 0.20	0.40 ± 0.19	0.36 ± 0.23
		18	1.07 ± 0.22	0.82 ± 0.15	0.48 ± 0.12	1.11 ± 0.28	0.93 ± 0.31	0.83 ± 0.34
		30	1.11 ± 0.24	0.74 ± 0.16	0.44 ± 0.12	1.57 ± 0.76	1.09 ± 0.41	0.93 ± 0.45
low	$\sigma_n = 0.01$	3	0.10 ± 0.03	0.07 ± 0.02	0.04 ± 0.01	0.38 ± 0.23	0.54 ± 0.26	0.38 ± 0.20
		18	0.48 ± 0.12	0.38 ± 0.09	0.27 ± 0.06	0.43 ± 0.13	0.35 ± 0.12	0.28 ± 0.11
		30	0.47 ± 0.11	0.30 ± 0.08	0.16 ± 0.04	0.45 ± 0.11	0.52 ± 0.23	0.32 ± 0.15
low	$\sigma_n = 0.03$	3	0.18 ± 0.06	0.13 ± 0.03	0.04 ± 0.01	0.68 ± 0.34	0.46 ± 0.23	0.31 ± 0.18
		18	1.00 ± 0.20	0.69 ± 0.15	0.27 ± 0.06	1.27 ± 0.36	1.47 ± 1.41	0.55 ± 0.16
		30	1.04 ± 0.28	0.65 ± 0.17	0.16 ± 0.04	1.40 ± 0.48	1.61 ± 1.40	0.66 ± 0.20

Table 2

The prediction error (MAE) of expected inhibitor accumulation fo hybrid model and LS.

Noise Level		Time (hrs)	Hybrid			LS		
b2b variation	process noise		$m = 3$	$m = 6$	$m = 20$	$m = 3$	$m = 6$	$m = 20$
high	$\sigma_n = 0.01$	3	0.13 ± 0.05	0.10 ± 0.03	0.06 ± 0.02	0.41 ± 0.20	0.59 ± 0.30	0.44 ± 0.22
		18	0.73 ± 0.19	0.49 ± 0.15	0.51 ± 0.11	1.82 ± 0.32	2.06 ± 0.26	2.09 ± 0.30
		30	1.23 ± 0.17	1.16 ± 0.12	1.12 ± 0.09	2.55 ± 0.33	2.53 ± 0.35	2.60 ± 0.41
high	$\sigma_n = 0.03$	3	0.20 ± 0.06	0.15 ± 0.04	0.08 ± 0.03	0.37 ± 0.20	0.40 ± 0.19	0.36 ± 0.24
		18	1.12 ± 0.25	0.88 ± 0.19	0.74 ± 0.16	1.78 ± 0.38	2.08 ± 0.27	2.23 ± 0.30
		30	1.33 ± 0.25	1.21 ± 0.20	1.22 ± 0.11	2.54 ± 0.41	2.79 ± 0.30	2.74 ± 0.35
low	$\sigma_n = 0.01$	3	0.10 ± 0.03	0.07 ± 0.02	0.04 ± 0.01	0.38 ± 0.23	0.54 ± 0.26	0.39 ± 0.20
		18	0.52 ± 0.12	0.36 ± 0.10	0.34 ± 0.07	2.03 ± 0.27	2.84 ± 0.22	2.30 ± 0.22
		30	1.03 ± 0.14	1.07 ± 0.09	1.02 ± 0.08	2.90 ± 0.24	2.91 ± 0.23	2.95 ± 0.22
low	$\sigma_n = 0.03$	3	0.18 ± 0.05	0.13 ± 0.04	0.07 ± 0.02	0.68 ± 0.34	0.46 ± 0.23	0.31 ± 0.18
		18	1.04 ± 0.22	0.75 ± 0.17	0.62 ± 0.13	2.17 ± 0.30	2.15 ± 0.29	2.13 ± 0.28
		30	1.27 ± 0.24	1.15 ± 0.18	1.07 ± 0.11	2.63 ± 0.36	2.67 ± 0.30	2.68 ± 0.33

For our model, we use the mean of the predictive distributions as the point forecast estimator $\hat{\rho}_t$ and \hat{I}_t for cell density ρ_t and inhibitor concentration I_t at t -th time step respectively. We set the number of macro replications as 30 and test sample size $N = 1000$.

Tables 1 and 2 record the mean absolute (forecast) error (MAE) with 95% confidence interval (CI) at t -th hour, where the mean is defined as $E_s(t) = \frac{1}{30} \sum_{r=1}^{30} E_s(t, r)$, standard error is $SE_s(t) = \frac{1}{\sqrt{30}} \sqrt{\frac{1}{29} \sum_{r=1}^{30} (E_s(t, r) - E_s(t))^2}$. The results demonstrate that our method can provide significantly better prediction accuracy in all noise levels ($\sigma_n = 0.01, 0.03$) and sample sizes of "real-world" observations ($m = 3, 6, 20$).

6.4. Medium Full Exchange

In this section, we focus on finding the optimal time to fully exchange the medium with fresh medium. Execution of this action (exchanging medium) will immediately reset the

concentration of inhibitor I to its initial value (i.e., 0 in fresh medium). Let $I_t = a_t I_t$ represent the post-exchanged concentration of inhibitor. The medium replacement decision a_t is a binary variable: $a_t = 0$ denoting the full exchange of medium at step t ; $a_t = 1$, otherwise.

The total operational cost, denoted by C , includes the costs related to facility time and media,

$$C(T, M) = C_f T + C_m M, \quad (21)$$

where C_f is the per unit facility use time-cost, C_m is the per unit media cost, T is the total cell culture time (in hours), and M is the volume of the medium (L). As the time step $\Delta t = 3$ hours, to avoid confusion, we use H to represent the last time step/index of cell culture process and use T to represent the total cell culture time (in hour).

The reward function is defined by cell yield per cost — the efficiency of the system during the T hours (H time

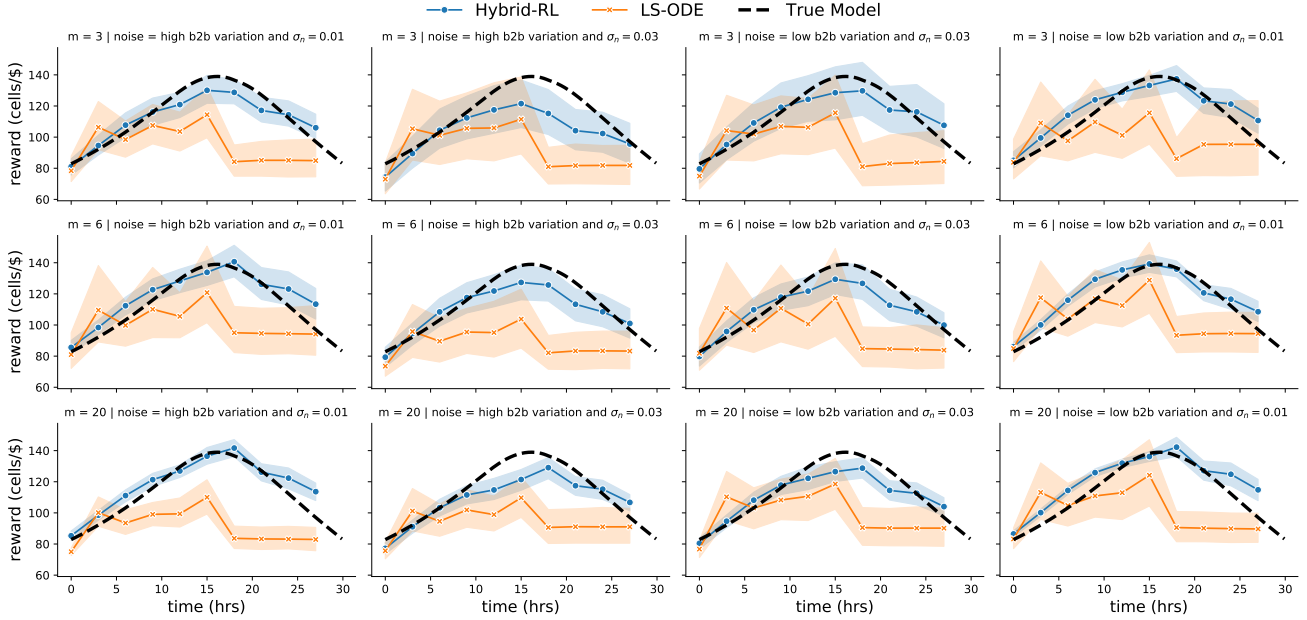


Figure 2: Performance comparison of hybrid model based reinforcement learning (hybrid-RL) and ODE mechanism model fitted by least square method (LS-ODE) in 30 macro-replications. The optimized reward with respect to the time of medium exchange are illustrated for hybrid-RL (point marker), LS-ODE (“x” marker) and “ground-truth” model (solid line). The validated models are used to optimize the media exchange time for cells to be produced with optimal cost efficiency given specified costs of cell culture medium and operational facility time at a given production scale (100L). The number of cells produced per dollar for a given time point of media exchange are calculated for any operating cost and consumable cost (here \$150/hr operating time cost and \$10/L of consumable cost per medium exchange).

Table 3

Medium exchange cost efficiency (cells/\$) of hybrid model based reinforcement learning and ODE mechanism model based brute-force screening approach. Cost efficiency are summarized as the mean (standard error) of cells per dollar across 30 macro-replications.

Noise Level		Hybrid-RL			LS-ODE		
batch-to-batch variation	process noise	$m = 3$	$m = 6$	$m = 20$	$m = 3$	$m = 6$	$m = 20$
high	$\sigma_n = 0.01$	115.07 (1.48)	117.99 (1.46)	121.64 (1.44)	111.11 (2.18)	108.67 (2.14)	112.67 (2.28)
high	$\sigma_n = 0.03$	113.74 (1.58)	114.81 (1.47)	114.58 (1.49)	111.11 (2.18)	114.40 (2.47)	108.85 (1.69)
low	$\sigma_n = 0.01$	115.74 (1.39)	119.16 (1.42)	122.17 (1.38)	110.12 (1.75)	111.52 (2.33)	112.70 (2.27)
low	$\sigma_n = 0.03$	114.98 (1.54)	115.19 (1.39)	116.00 (1.36)	111.25 (2.02)	111.87 (2.26)	110.66 (2.06)

steps) cell culture,

$$r_t = 0 \quad \text{with} \quad 0 \leq t \leq H$$

$$r_{H+1}(\mathbf{s}_{H+1}, a_{H+1} = \text{“Harvest”}) = \frac{M(\rho_T - \rho_0)}{C(T, M)}$$

where ρ_T represents the cell density at T -th hour. As it is certainly suboptimal to exchange medium at harvest time (30th hour), we only consider step $t \leq 10$ since $\Delta t = 3$ hours. Then the optimal timing of media exchange can be obtained by Algorithm 2. We set the harvest time as 30 hours ($T = 30$ corresponding to time step $t = 11$) and the medium is fully exchanged up to 1 time in decision hours $\{0, 3, \dots, 27\}$.

Following the study in Glen et al. (2018), we consider an exchange time optimization problem where cells per cost is calculated for running a 100L bioreactor from the starting density $3 \times 10^6/\text{mL}$ with hypothetical facility and equipment operating costs of \$150/hr and cell culture medium costs of \$10/L. We solve this problem by using the proposed hybrid model based reinforcement learning (hybrid-RL) and the ODE-based mechanistic model fitted by least square method (LS-ODE). We compare their performance in the situations with different levels of variations and different sample sizes (i.e., m) of the “ground-truth” cell culture process observations. Similar to Glen et al. (2018), the

Table 4

Culture expansion profit (\$) of hybrid-RL and ODE mechanism model based brute-force screening approach. Profit are summarized as the mean (standard error) of dollar across 30 macro-replications.

Noise Level		Hybrid-RL			LS-ODE		
batch-to-batch variation	process noise	$m = 3$	$m = 6$	$m = 20$	$m = 3$	$m = 6$	$m = 20$
high	$\sigma_n = 0.01$	7317.24 (352.37)	7588.15 (322.53)	7892.84 (69.65)	5677.62 (389.24)	5944.25 (403.52)	6030.83 (399.61)
high	$\sigma_n = 0.03$	6888.86 (693.07)	7266.23 (393.66)	7689.45 (143.11)	-2259.01 (704.82)	1026.60 (484.50)	2454.22 (262.15)
low	$\sigma_n = 0.01$	7800.60 (151.01)	7955.38 (75.78)	8035.71 (52.48)	6115.31 (413.23)	6193.70 (381.83)	6417.39 (389.06)
low	$\sigma_n = 0.03$	7414.34 (334.41)	7572.99 (329.62)	7974.35 (76.15)	5978.52 (389.96)	6126.60 (393.61)	6225.02 (395.50)

optimization of LS-ODE was performed via an exhaustive search of decision space.

We illustrate the cost efficiency of full medium exchange at each decision time across different levels of uncertainty and sample size in Figure 2. The markers represent the rewards/cost efficiencies at the corresponding decision time and the translucent bands around marks are the 95% confidence intervals estimated by bootstrapping. The results are obtained based on 30 macro-replications. The cost efficiency curves estimated by LS-ODE have large discrepancies to those from “ground-truth” model and they have significantly wider confidence bands, indicating that this model suffers from the high variation between macro-replications. In addition, we observe that hybrid-RL has a shrinking trend of the confidence intervals as the sample size m increases.

We summarize the performance of optimal decisions obtained from hybrid-RL and LS-ODE approaches in Table 3. Overall, hybrid-RL outperforms LS-ODE (with higher reward/cost efficiency) in all different levels of variations and sample sizes. It shows a strong evidence that hybrid-RL is more robust than the regular deterministic mechanistic model fitted by least-square method. Another interesting observation is that the optimal medium exchange decisions obtained by LS-ODE are not as bad as the estimated cost efficiency curve in Figure 2. It is because the response curve is relative flat (range from 104 cells/\$ to 167 cells/\$). To further evaluate the performance, we consider another optimization problem, “cell culture expansion” with the same simulated data and process models used in Section 6.5.

6.5. Cell Culture Expansion

In this section, we focus on optimizing the number and timing of cell expansions. For each expansion, the original batch is scaled up to a n times larger cell culture vessel filling with fresh medium. The cell density ρ and the concentration of inhibitor I decrease to $1/n$ of original batch immediately after each scale-up. If the culture expansion action is taken, that is $a_t = 1$, then the post-exchanged cell density becomes $\rho_t = \frac{1}{n}\rho_t$ and post-exchanged inhibitor $I_t = \frac{1}{n}I_t$; otherwise,

$a_t = 0$. The cell culture scale-up problem can be solved by Algorithm 2. The expansion decision can be made every 3 hours starting from the third hour until the harvest time at 30-th hour ($T = 30$). Thus the maximal number of potential culture expansions is 9 when expansion decisions are made in all decision hours.

In terms of the reward function, we use the same total operational cost as presented in Section 6.4, and further introduce the revenue of cell therapy production based on unit price of cells denoted by P_c as follows

$$K(\rho_T, \xi, n) = P_c \times \rho_T \times n^\xi$$

where ξ is the total number of cell culture expansion and ρ_T is the cell density at harvest hour T . Here we set expansion scale $n = 4$ and set the price $P_c = \$2 \times 10^{-6}$ per cell.

The reward function is then defined by the difference between revenue and cost as,

$$\begin{aligned} r_t &= 0 \text{ with } 0 \leq t \leq H \\ r_{H+1} &(\mathbf{s}_{H+1}, \mathbf{a}_{H+1} = \text{“Harvest”}) \\ &= K(\rho_T, \xi, n) - C(T, M) \end{aligned}$$

where $C(T, M)$ is defined by (21). In this case, we expand the culture in a 1L seed bioreactor multiple times to achieve maximal profit. We set the initial cell density as $3 \times 10^6/\text{mL}$, hypothetical facility and equipment operating costs as \$150/hr and cell culture medium costs as \$10/L.

We summarize the performance of hybrid-RL and LS-ODE methods in the situations with different noise levels and samples in Table 4. It shows a strong evidence that hybrid-RL provides significantly better and more robust expansion decisions compared to LS-ODE. In all these settings, the mean profit of hybrid-RL obtained from 30 macro-replications are all greater than 6000 dollars. Comparatively, the performance of LS-ODE method, with profits below 6,500 dollars in all cases, is significantly worse than hybrid model especially in the case with high batch-to-batch variation and process noise.

To better understand the optimality gap, we performed a side experiment to calculate the true optimal profit based

on the “ground-truth” simulation model and conduct the exhaustive search of all possible combinations of actions (2^9 different combinations) to find the optimal expansion decision. As a result, the true optimal action is found to be running one expansion at the 6-th hour (from 1 L to 4 L) with the corresponding maximal profit \$8593.85. By comparing the mean profit of hybrid-RL with the true expected optimal profit, it shows that the optimality gap of hybrid-RL is consistently lower than LS-ODE. Evidently, the largest gap \$1704.99 occurs at the situation with high stochastic uncertainty (i.e., $\sigma_n = 0.03$) and high model uncertainty (i.e., $m = 3$). The smallest gap \$558.14 occurs at the situation with low stochastic and model uncertainties, i.e., low noise and large sample size.

7. Conclusions

The cell therapy manufacturing stochastic uncertainty (i.e., batch-to-batch variation and bioprocess noise) is often overlooked by the current mechanistic model literature. This can lead to sub-optimal and unreliable decision making. Thus, we introduce a probabilistic knowledge graph that is a hybrid model characterizing complex interactions of various sources of uncertainties and mechanism pathways connecting CPPs/CQAs. It can leverage on the information from existing PDE/ODE-based mechanistic models and facilitate the learning from process data. This hybrid model can capture the important properties of integrated biomanufacturing processes, including nonlinear reactions, partially observed state, and time-varying kinetics.

To efficiently support process development and control, we create a hybrid model-based reinforcement learning accounting for both inherent stochasticity and model uncertainty. It can provide an insightful and reliable prediction on how the effects of inputs propagate through bioprocessing mechanism pathways and impact on the output trajectory dynamics and variation. Therefore, the proposed hybrid-RL framework can find optimal, robust, and interpretable decisions and control policies, which can overcome the key challenges of cell therapy manufacturing, i.e., high complexity, high uncertainty, and very limited process data. The empirical study demonstrates that the proposed framework can outperform the classical approach, especially under the situations with high inherent stochasticity and limited historical data which induces high model uncertainty.

Acknowledgements

We acknowledge Richard D. Braatz (from Massachusetts Institute of Technology) for his insightful discussion and constructive feedback on this study.

References

Almquist, J., Cvijovic, M., Hatzimanikatis, V., Nielsen, J., Jirstrand, M., 2014. Kinetic models in industrial biotechnology—improving cell factory performance. *Metabolic engineering* 24, 38–60.

Bayram, M., Partal, T., Buyukoz, G.O., 2018. Numerical methods for simulation of stochastic differential equations. *Advances in Difference Equations* 2018, 1–10.

Beaumont, M.A., Cornuet, J.M., Marin, J.M., Robert, C.P., 2009. Adaptive approximate bayesian computation. *Biometrika* 96, 983–990.

Blanchini, F., El-Samad, H., Giordano, G., Sontag, E.D., 2018. Control-theoretic methods for biological networks, in: *Proc. 2018 IEEE Conf. Decision and Control*, pp. 466–483.

Bollas, G., Papadokonstadakis, S., Michalopoulos, J., Arampatzis, G., Lappas, A., Vasalos, I., Lygeros, A., 2003. Using hybrid neural networks in scaling up an fcc model from a pilot plant to an industrial unit. *Chemical Engineering and Processing: Process Intensification* 42, 697–713.

Dickens, J., Khattak, S., Matthews, T.E., Kolwyck, D., Wiltberger, K., 2018. Biopharmaceutical raw material variation and control. *Current opinion in chemical engineering* 22, 236–243.

Fiorenza, S., Ritchie, D.S., Ramsey, S.D., Turtle, C.J., Roth, J.A., 2020. Value and affordability of car t-cell therapy in the united states. *Bone marrow transplantation* 55, 1706–1715.

Ghavamzadeh, M., Mannor, S., Pineau, J., Tamar, A., 2016. Bayesian reinforcement learning: A survey. *arXiv preprint arXiv:1609.04436*.

Glen, K.E., Cheeseman, E.A., Stacey, A.J., Thomas, R.J., 2018. A mechanistic model of erythroblast growth inhibition providing a framework for optimisation of cell therapy manufacturing. *Biochemical Engineering Journal* 133, 28–38.

Gunther, J.C., Conner, J.S., Seborg, D.E., 2009. Process monitoring and quality variable prediction utilizing pls in industrial fed-batch cell culture. *Journal of Process Control* 19, 914–921.

Hanna, E., Rémuzat, C., Auquier, P., Toumi, M., 2016. Advanced therapy medicinal products: current and future perspectives. *Journal of market access & health policy* 4, 31036.

Hong, M.S., Severson, K.A., Jiang, M., Lu, A.E., Love, J.C., Braatz, R.D., 2018. Challenges and opportunities in biopharmaceutical manufacturing control. *Computers & Chemical Engineering* 110, 106–114.

Jiang, M., Braatz, R., 2016. Integrated control of continuous (bio) pharmaceutical manufacturing. *American Pharmaceutical Review* 19, 110–115.

Jin, C., Yang, Z., Wang, Z., Jordan, M.I., 2020. Provably efficient reinforcement learning with linear function approximation, in: *Conference on Learning Theory*, PMLR. pp. 2137–2143.

Kearns, M., Mansour, Y., Ng, A.Y., 2002. A sparse sampling algorithm for near-optimal planning in large markov decision processes. *Machine learning* 49, 193–208.

Kee, N.C., Tan, R.B., Braatz, R.D., 2009. Selective crystallization of the metastable α -form of l-glutamic acid using concentration feedback control. *Crystal Growth and Design* 9, 3044–3051.

Kirdar, A.O., Conner, J.S., Baclaski, J., Rathore, A.S., 2007. Application of multivariate analysis toward biotech processes: case study of a cell-culture unit operation. *Biotechnology progress* 23, 61–67.

Knappert, J., McHardy, C., Rauh, C., 2020. Kinetic modeling and numerical simulation as tools to scale microalgae cell membrane permeabilization by means of pulsed electric fields (pef) from lab to pilot plants. *Frontiers in bioengineering and biotechnology* 8, 209.

Kocijan, J., Murray-Smith, R., Rasmussen, C.E., Girard, A., 2004. Gaussian process model based predictive control, in: *Proceedings of the 2004 American Control Conference*, pp. 2214–2219 vol.3. doi:10.23919/ACC.2004.1383790.

Lakerveld, R., Benyahia, B., Braatz, R.D., Barton, P.I., 2013. Model-based design of a plant-wide control strategy for a continuous pharmaceutical plant. *AIChE Journal* 59, 3671–3685.

Lenormand, M., Jabot, F., Deffuant, G., 2013. Adaptive approximate bayesian computation for complex models. *Computational Statistics* 28, 2777–2796.

Liu, C., Gong, Z., Shen, B., Feng, E., 2013. Modelling and optimal control for a fed-batch fermentation process. *Applied Mathematical Modelling* 37, 695–706.

Lu, A.E., Paulson, J.A., Mozdzier, N.J., Stockdale, A., Versypt, A.N.F., Love, K.R., Love, J.C., Braatz, R.D., 2015. Control systems technology in the advanced manufacturing of biologic drugs, in: *Proceedings of the IEEE Conference on Control Applications*, pp. 1505–1515.

- Machalek, D., Quah, T., Powell, K.M., 2021. A novel implicit hybrid machine learning model and its application for reinforcement learning. *Computers & Chemical Engineering* 155, 107496.
- Malham, S.J., Wiese, A., 2010. An introduction to sde simulation. arXiv preprint arXiv:1004.0646.
- Mandenius, C.F., Titchener-Hooker, N.J., et al., 2013. Measurement, monitoring, modelling and control of bioprocesses. volume 132. Springer.
- Martagan, T., Krishnamurthy, A., Leland, P.A., Maravelias, C.T., 2017. Performance guarantees and optimal purification decisions for engineered proteins. *Operations Research* 66, 18–41.
- Martagan, T., Krishnamurthy, A., Leland, P.A., Maravelias, C.T., 2018. Performance guarantees and optimal purification decisions for engineered proteins. *Operations Research* 66, 18–41.
- McDonald, K., Ho, K., 2012. Ich q11: development and manufacture of drug substances—chemical and biotechnological/biological entities. *Generics and Biosimilars Initiative Journal* 1, 142–144.
- McKinley, T.J., Vernon, I., Andrianakis, I., McCreesh, N., Oakley, J.E., Nsubuga, R.N., Goldstein, M., White, R.G., 2018. Approximate bayesian computation and simulation-based inference for complex stochastic epidemic models. *Statistical science* 33, 4–18.
- Mercier, S.M., Diepenbroek, B., Dalm, M.C., Wijffels, R.H., Streefland, M., 2013. Multivariate data analysis as a pat tool for early bioprocess development data. *Journal of biotechnology* 167, 262–270.
- Mesbah, A., Paulson, J.A., Lakerveld, R., Braatz, R.D., 2017. Model predictive control of an integrated continuous pharmaceutical manufacturing pilot plant. *Organic Process Research & Development* 21, 844–854.
- Minter, A., Retkute, R., 2019. Approximate bayesian computation for infectious disease modelling. *Epidemics* 29, 100368.
- Mockus, L., Peterson, J.J., Lainez, J.M., Reklaitis, G.V., 2015. Batch-to-batch variation: a key component for modeling chemical manufacturing processes. *Organic Process Research & Development* 19, 908–914.
- Mowbray, M., Petsagkourakis, P., del Rio-Chanona, E., Zhang, D., 2021. Safe chance constrained reinforcement learning for batch process control. *Computers & Chemical Engineering*, 107630 URL: <https://www.sciencedirect.com/science/article/pii/S0098135421004087>, doi:<https://doi.org/10.1016/j.compchemeng.2021.107630>.
- Nfor, B.K., Verhaert, P.D.E.M., van der Wielen, L.A.M., Hubbuch, J., Otens, M., 2009. Rational and systematic protein purification process development: the next generation. *Trends in Biotechnology* 27, 673–679.
- Pan, E., Petsagkourakis, P., Mowbray, M., Zhang, D., del Rio-Chanona, E.A., 2021. Constrained model-free reinforcement learning for process optimization. *Computers & Chemical Engineering* 154, 107462.
- Paulson, J.A., Streif, S., Findeisen, R., Braatz, R.D., Mesbah, A., 2018. Fast stochastic model predictive control of end-to-end continuous pharmaceutical manufacturing, in: Singh, R., Yuan, Z. (Eds.), *Process Systems Engineering for Pharmaceutical Manufacturing*. Elsevier, Amsterdam, Netherlands. chapter 14, pp. 353–378.
- Puterman, M.L., 2014. *Markov decision processes: discrete stochastic dynamic programming*. John Wiley & Sons.
- Rain-Franco, A., De Moraes, G.P., Beier, S., 2021. Cryopreservation and resuscitation of natural aquatic prokaryotic communities. *Frontiers in microbiology*, 3633.
- Silver, D., Huang, A., Maddison, C.J., Guez, A., Sifre, L., Van Den Driessche, G., Schrittwieser, J., Antonoglou, I., Panneershelvam, V., Lanctot, M., et al., 2016. Mastering the game of go with deep neural networks and tree search. *nature* 529, 484–489.
- Solle, D., Hitzmann, B., Herwig, C., Pereira Remelhe, M., Ulonka, S., Wuerth, L., Prata, A., Steckenreiter, T., 2017. Between the poles of data-driven and mechanistic modeling for process operation. *Chemie Ingenieur Technik* 89, 542–561.
- Spielberg, S., Gopaluni, R., Loewen, P., 2017. Deep reinforcement learning approaches for process control, in: 2017 6th international symposium on advanced control of industrial processes (AdCONIP), IEEE. pp. 201–206.
- Spielberg, S., Tulsyan, A., Lawrence, N.P., Loewen, P.D., Gopaluni, R.B., 2020. Deep reinforcement learning for process control: A primer for beginners. arXiv preprint arXiv:2004.05490.
- Steinwandter, V., Borchert, D., Herwig, C., 2019. Data science tools and applications on the way to pharma 4.0. *Drug discovery today* 24, 1795–1805.
- von Stosch, M., Hamelink, J.M., Oliveira, R., 2016. Hybrid modeling as a qbd/pat tool in process development: an industrial e. coli case study. *Bioprocess and biosystems engineering* 39, 773–784.
- Teixeira, A.P., Carinhas, N., Dias, J.M.L., Cruz, P., Alves, P.M., Carrondo, M.J.T., Oliveira, R., 2007. Hybrid semi-parametric mathematical systems: Bridging the gap between systems biology and process engineering. *Journal of Biotechnology* 132, 418–425.
- Teixeira, A.P., Portugal, C.A., Carinhas, N., Dias, J.M., Crespo, J.P., Alves, P.M., Carrondo, M., Oliveira, R., 2009. In situ 2d fluorometry and chemometric monitoring of mammalian cell cultures. *Biotechnology and bioengineering* 102, 1098–1106.
- Toni, T., Welch, D., Strelkowa, N., Ipsen, A., Stumpf, M.P., 2009. Approximate bayesian computation scheme for parameter inference and model selection in dynamical systems. *Journal of the Royal Society Interface* 6, 187–202.
- Treloar, N.J., Fedorec, A.J., Ingalls, B., Barnes, C.P., 2020. Deep reinforcement learning for the control of microbial co-cultures in bioreactors. *PLoS computational biology* 16, e1007783.
- Vasdekis, A., Silverman, A.M., Stephanopoulos, G., 2015. Origins of cell-to-cell bioprocessing diversity and implications of the extracellular environment revealed at the single-cell level. *Scientific Reports* 5, 1–7.
- von Stosch, M., Oliveira, R., Peres, J., Feyo de Azevedo, S., 2014. Hybrid semi-parametric modeling in process systems engineering: Past, present and future. *Computers & Chemical Engineering* 60, 86–101. URL: <https://www.sciencedirect.com/science/article/pii/S0098135413002639>, doi:<https://doi.org/10.1016/j.compchemeng.2013.08.008>.
- Wang, B., Xie, W., Martagan, T., Akcay, A., van Ravenstein, B., 2021a. Optimizing biomanufacturing harvesting decisions under limited historical data. arXiv preprint arXiv:2101.03735.
- Wang, L.L.W., Janes, M.E., Kumbhokar, N., Kapate, N., Clegg, J.R., Prakash, S., Heavey, M.K., Zhao, Z., Anselmo, A.C., Mitravotri, S., 2021b. Cell therapies in the clinic. *Bioengineering & translational medicine* 6, e10214.
- Wang, T., Lizotte, D., Bowling, M., Schuurmans, D., 2005. Bayesian sparse sampling for on-line reward optimization, in: *Proceedings of the 22nd international conference on Machine learning*, pp. 956–963.
- Xie, W., Wang, B., Li, C., Xie, D., Auclair, J., 2020. Interpretable biomanufacturing process risk and sensitivity analyses for quality-by-design and stability control. *Naval Research Logistics (NRL)* URL: <https://onlinelibrary.wiley.com/doi/abs/10.1002/nav.22019>, doi:<https://doi.org/10.1002/nav.22019>.
- Zhang, S., Wang, F., He, D., Jia, R., 2012. Batch-to-batch control of particle size distribution in cobalt oxalate synthesis process based on hybrid model. *Powder technology* 224, 253–259.
- Zheng, H., Ryzhov, I.O., Xie, W., Zhong, J., 2021a. Personalized multimorbidity management for patients with type 2 diabetes using reinforcement learning of electronic health records. *Drugs* URL: <https://doi.org/10.1007/s40265-020-01435-4>, doi:10.1007/s40265-020-01435-4.
- Zheng, H., Xie, W., Ryzhov, I.O., Xie, D., 2021b. Policy optimization in bayesian network hybrid models of biomanufacturing processes. arXiv:2105.06543.